

Mettle: Meta-Token Learning for Memory-Efficient Audio-Visual Adaptation

Jinxing Zhou¹, Zhihui Li^{3,*}, Yongqiang Yu¹, Yanghao Zhou⁴, Ruohao Guo⁵, Guangyao Li⁶,
Yuxin Mao⁷, Mingfei Han¹, Xiaojun Chang^{1,3}, Meng Wang^{2,*}

¹MBZUAI ²Hefei University of Technology ³University of Science and Technology of China
⁴National University of Singapore ⁵Peking University ⁶Tsinghua University ⁷OpenNLP Lab

Abstract

Mainstream research in audio-visual learning has focused on designing task-specific expert models, primarily implemented through sophisticated multimodal fusion approaches. Recently, a few efforts have aimed to develop more task-independent or universal audiovisual embedding networks, encoding advanced representations for use in various audiovisual downstream tasks. This is typically achieved by fine-tuning large pretrained transformers, such as Swin-V2-L and HTS-AT, in a parameter-efficient manner through techniques such as tuning only a few *adapter* layers inserted into the pretrained transformer backbone. Although these methods are parameter-efficient, they suffer from significant training memory consumption due to gradient backpropagation through the deep transformer backbones, which limits accessibility for researchers with constrained computational resources. In this paper, we present **Meta-Token Learning** (Mettle), a simple and memory-efficient method for adapting large-scale pretrained transformer models to downstream audio-visual tasks. Instead of sequentially modifying the output feature distribution of the transformer backbone, Mettle utilizes a lightweight *Layer-Centric Distillation (LCD)* module to distill in parallel the intact audio or visual features embedded by each transformer layer into compact meta-tokens. This distillation process considers both pretrained knowledge preservation and task-specific adaptation. The obtained meta-tokens can be directly applied to classification tasks, such as audio-visual event localization and audio-visual video parsing. To further support fine-grained segmentation tasks, such as audio-visual segmentation, we introduce a *Meta-Token Injection (MTI)* module, which utilizes the audio and visual meta-tokens distilled from the top transformer layer to guide feature adaptation in earlier layers. Extensive experiments on multiple audiovisual benchmarks demonstrate that our method significantly reduces memory usage and training time while maintaining parameter efficiency and competitive accuracy.

1 Introduction

Audio-visual learning [Wei et al. \(2022\)](#) has received increasing attention in recent years, aiming to enable machines to mimic human intelligence in processing and analyzing complex audiovisual signals from real-world scenarios. Prior studies primarily focus on developing specialized expert models for individual audiovisual learning tasks, such as classification [Tian et al. \(2018b, 2020\)](#) and segmentation [Zhou et al. \(2022b\)](#) problems. To enhance these tasks, various task-oriented modules have been proposed to improve the audio-visual *late* fusion [Lin et al. \(2019\)](#); [Zhou et al. \(2021\)](#); [Xu et al. \(2020\)](#); [Xia & Zhao \(2022\)](#); [Yu et al. \(2022\)](#); [Tian et al. \(2020\)](#); [Mo & Tian \(2022\)](#); [Zhou et al. \(2022b\)](#); [Li et al. \(2023b\)](#).

Recent advances [Lin et al. \(2023\)](#); [Duan et al. \(2024\)](#); [Cheng et al. \(2024\)](#) in audio-visual learning aim to enhance more task-universal *early* audiovisual feature encoding stage by fine-tuning large-scale pre-trained transformer backbones (*e.g.*, ViT-L-16 [Dosovitskiy \(2021\)](#) and Swin-V2-L [Liu et al. \(2022\)](#)) using a *parameter-efficient* paradigm. As shown in Figure 1a, mainstream parameter-efficient methods, such as LAVisH [Lin et al. \(2023\)](#), DG-SCT [Duan et al. \(2024\)](#), and AVMoE [Cheng et al. \(2024\)](#), typically insert

* Corresponding authors (lizhihuics@ustc.edu.cn, eric.mengwang@gmail.com)

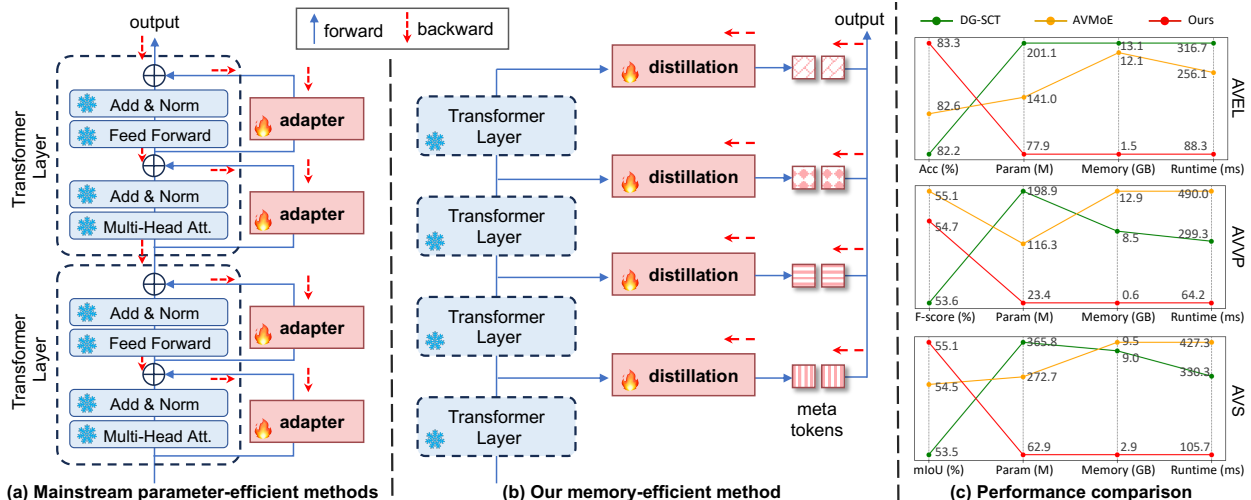


Figure 1. (a) Mainstream parameter-efficient methods for audiovisual adaptation insert learnable adapters within each frozen transformer layer. This alters the original feature output, inducing heavy memory overhead during backpropagation. (b) The core idea of our memory-efficient method aims to generate compact meta-tokens via parallel distillation from each transformer layer, preventing gradient propagation through the transformer backbone. (c) Comparison with prior state-of-the-art methods (e.g., DG-SCT Duan et al. (2024) and AVMoE Cheng et al. (2024)) in terms of accuracy, trainable parameters, memory and runtime during training on the AVEL Tian et al. (2018b), AVVP Tian et al. (2020), and AVS Zhou et al. (2022b) tasks. The multi-source setting of AVS is illustrated. Swin-V2-L Liu et al. (2022) and HTS-AT Chen et al. (2022b) are used as the visual and audio transformer backbones, respectively. Memory and runtime values represent the per-sample consumption during model training (i.e., batch size = 1).

adapter Houshy et al. (2019) layers into the residual connection branch of each transformer layer. These adapter layers are designed to learn task-related representations for downstream tasks. Since the parameters of the pretrained transformer layers remain frozen while only the inserted adapter layers are trainable, these methods ensure parameter efficiency. However, they suffer from *memory inefficiency*. As illustrated in Figure 1a, the output of each transformer layer is changed and gradients need to be propagated through the entire model to update adapter parameters. This leads to substantial memory overhead and significantly increased optimization time during training. For example, the prior state-of-the-art AVMoE Cheng et al. (2024) requires 12.1GB of GPU memory for training on the AVE Tian et al. (2018b) dataset, even with a batch size of 1. Such limitation prohibits the use of larger batch sizes for faster training and poses challenges for researchers with constrained computational resources.

In this paper, we explore *memory-efficient audio-visual adaptation*, which aims to adapt large-scale pretrained transformer models for downstream audiovisual learning tasks in a memory-efficient manner, while maintaining parameter efficiency and competitive accuracy. The memory inefficiency of prior models Lin et al. (2023); Duan et al. (2024); Cheng et al. (2024) arises from the *sequential* processing of intermediate transformer features from bottom to top layers. We consider enforcing the model learning process in *parallel* with transformer layers. Since transformer backbones comprising deep layers are pretrained on large datasets, they can capture generalizable patterns and structural regularities in feature embedding Raghu et al. (2021); Cordonnier et al. (2020). Thus, the encoded intermediate features retain useful information, allowing them to be directly and layer-independently leveraged for downstream adaptation.

Motivated by this, we propose a **Layer-Centric Distillation (LCD)** module, which aims to distill useful representations from each pretrained transformer layer into a set of **meta-tokens**, as illustrated in Figure 1b. We refer to them as *meta*-tokens because they are highly compact, with significantly fewer elements than the source audio or visual tokens embedded by pretrained transformer layers. Specifically, the meta-tokens are first initialized as learnable vectors and then updated through iterative distillation from pretrained modality-specific tokens. LCD performs this distillation through two key mechanisms (see Figure 2a). First, the learnable meta-tokens interact with pretrained audio/visual tokens by modeling their cross-attentions [Dosovitskiy \(2021\)](#), querying task-relevant representations to refine the meta-tokens; Meanwhile, a lightweight linear layer is directly applied to the original audio/visual tokens to better preserve effective pretrained knowledge. Afterward, the obtained meta-tokens from different transformer layers are aggregated to comprehensively leverage diverse representations captured across layers. This aggregation is implemented using parameter-free average pooling, yielding ultimate meta-tokens for downstream adaptation. We apply LCD separately to the audio or visual modality to generate *early* audio/visual meta-tokens. Existing sophisticated audio-visual interaction strategies can then be incorporated at *late* stage to generate predictions for downstream tasks [Duan et al. \(2024\)](#); [Cheng et al. \(2024\)](#).

We dub this approach as ***Meta-Token Learning (Mettle)***, where the learned meta-tokens can be directly used for downstream classification tasks in audio-visual learning, such as audio-visual event localization (AVEL) [Tian et al. \(2018b\)](#) and audio-visual video parsing (AVVP) [Tian et al. \(2020\)](#). Furthermore, we extend *Mettle* to more complex segmentation tasks, such as audio-visual segmentation (AVS) [Zhou et al. \(2022b\)](#). For such tasks, it is infeasible to generate pixel-level predictions solely from compact audio or visual meta-tokens. We further propose the **Meta-Token Injection (MTI)** module, which reintegrates the distilled knowledge in meta-tokens into visual tokens (higher-resolution flattened features maps) encoded by pretrained transformers (illustrated in Figure 2b). Specifically, we apply the LCD module only to the final layer of the pretrained transformer backbone to obtain audio and visual meta-tokens containing high-level semantics. These meta-tokens are then injected into the visual tokens from earlier layers through cross-modal and intra-modal dot-product attention [Vaswani et al. \(2017\)](#) modeling. This process allows the hidden knowledge captured by audio or visual meta-tokens to enhance the representations of pretrained visual tokens, directing them toward task-related adaptations (*e.g.*, highlighting audio-driven regions of interest in AVS task).

Our *Mettle* approach avoids gradient backpropagation along the large transformer backbone, ensuring memory efficiency. Moreover, the LCD module and the MTI module inserted into the transformer layer(s) are deliberately designed to be simple and lightweight, requiring only minimal learnable parameters. As a result, our model is both parameter- and memory-efficient. We conduct extensive experiments on three representative audio-visual downstream tasks: AVEL [Tian et al. \(2018b\)](#), AVVP [Tian et al. \(2020\)](#), and AVS [Zhou et al. \(2022b\)](#). Figure 1c provides a comprehensive comparison of our method with prior parameter-efficient works [Duan et al. \(2024\)](#); [Cheng et al. \(2024\)](#). Our method achieves competitive or superior accuracy while significantly reducing the consumption of trainable parameters, training memory, and runtime. For example, on the AVEL task, our method outperforms prior state-of-the-art AVMoE [Cheng et al. \(2024\)](#) by 0.7% in accuracy, while using **45%** fewer trainable parameters, **88%** less memory, and **65%** less training runtime.

To summarize, our main contributions are threefold:

- We propose *Mettle*, the first memory-efficient framework for adapting large-scale pretrained transformers to downstream audio-visual learning tasks.

- We introduce lightweight technical designs, including the Layer-Centric Distillation (LCD) and Meta-Token Injection (MTI), highlighting compact meta-token learning and utilization.
- We achieve superior performance across multiple audio-visual classification and segmentation benchmarks, maintaining competitive accuracy while ensuring high efficiency in parameters, memory usage, and training time.

2 Related Work

2.1 Audio-Visual Learning

Audio-Visual Learning has made significant progress in recent years, with studies covering a range of tasks, such as classification [Arandjelovic & Zisserman \(2018\)](#); [Cheng et al. \(2020\)](#); [Tian et al. \(2018b, 2020\)](#); [Zhou et al. \(2025c\)](#); [Liu et al. \(2025\)](#), detection [Zhao et al. \(2018\)](#); [Chen et al. \(2021\)](#); [Hu et al. \(2020\)](#); [Mahmud et al. \(2024b\)](#), segmentation [Zhou et al. \(2022b, 2023b\)](#); [Guo et al. \(2024b, 2025\)](#), and text-involved captioning [Tian et al. \(2018a\)](#); [Shen et al. \(2023\)](#); [Tian et al. \(2019\)](#); [Mao et al. \(2024\)](#); [Kim et al. \(2024\)](#) or question answering [Yun et al. \(2021\)](#); [Li et al. \(2022, 2024b, 2023a, 2024a, 2025\)](#) tasks. In this work, we focus on three key audiovisual tasks. The *Audio-Visual Event Localization (AVEL)* [Tian et al. \(2018b\)](#); [Lin et al. \(2019\)](#); [Zhou et al. \(2021, 2022a\)](#); [Lin & Wang \(2020\)](#); [Rao et al. \(2022\)](#); [Xia & Zhao \(2022\)](#); [Zhou et al. \(2025a\)](#) task aims to identify temporal segments where both audible and visible events occur, providing a fundamental understanding of audio-visual correspondence. Since audio and visual signals are not always temporally or spatially aligned (*e.g.*, the sounding objects may be out-of-view), researchers have further explored the *Audio-Visual Video Parsing (AVVP)* [Tian et al. \(2020\)](#); [Wu & Yang \(2021\)](#); [Cheng et al. \(2022\)](#); [Gao et al. \(2023a\)](#); [Lai et al. \(2023\)](#); [Sardari et al. \(2024\)](#); [Zhou et al. \(2023a, 2024a,b\)](#); [Zhao et al. \(2025\)](#) task. Unlike AVEL, AVVP not only detects audio-visual events but also distinguishes events that are exclusively audible or visible. Beyond these temporal classification tasks, the *Audio-Visual Segmentation (AVS)* [Zhou et al. \(2022b\)](#); [Li et al. \(2023b\)](#); [Gao et al. \(2024\)](#); [Liu et al. \(2024\)](#); [Guo et al. \(2024a\)](#); [Ma et al. \(2024\)](#); [Chen et al. \(2024\)](#); [Zhou et al. \(2025b\)](#) task focuses on the spatial comprehension of audiovisual scenes by generating pixel-level masks of sounding objects. Traditional methods for these tasks primarily focus on the *late* fusion of extracted audiovisual features. In contrast, our work enhances *early* feature encoding by adapting rich representations from large-scale pretrained transformers.

2.2 Parameter-Efficient Transfer Learning

Parameter-Efficient Transfer Learning (PETL) aims to adapt large pretrained foundation models to downstream tasks by fine-tuning only a small subset of parameters. Initially developed in the natural language processing (NLP) domain, PETL techniques include inserting lightweight adapter layers [Houlsby et al. \(2019\)](#); [Bapna et al. \(2019\)](#); [Karimi Mahabadi et al. \(2021\)](#), learning low-rank adaptation of tunable weights [Hu et al. \(2021\)](#), and prepending learnable prompts to the input sequence [Lester et al. \(2021\)](#); [Gu et al. \(2021\)](#); [Li & Liang \(2021\)](#). PETL has demonstrated the ability to achieve comparable or even better performance than full fine-tuning while significantly reducing the number of trainable parameters. This success has inspired extensive studies in computer vision [Zhu et al. \(2023\)](#); [Jia et al. \(2022\)](#); [Gao et al. \(2023b\)](#); [Park & Byun \(2024\)](#); [Yang et al. \(2024\)](#); [Wang et al. \(2024b\)](#) and vision-language [Chen et al. \(2022a\)](#); [Huang et al. \(2023\)](#); [Khattak et al. \(2023a\)](#); [Zhou et al. \(2022c\)](#); [Roy & Etemad \(2023\)](#); [Khattak et al. \(2023b\)](#); [Zhang et al. \(2024\)](#); [Yao et al. \(2024\)](#) domains.

In the field of audiovisual learning, Lin *et al.* introduced LAVisH Lin *et al.* (2023), which transfers knowledge from pretrained vision transformers (*e.g.*, ViT Dosovitskiy (2021) and Swin-Transformer Liu *et al.* (2022)) to downstream audiovisual tasks. LAVisH keeps vision transformers frozen and fine-tunes only cross-modal adapters inserted into each transformer layer. Subsequent works have explored improved cross-modal interactions using more advanced adapters Duan *et al.* (2024); Cheng *et al.* (2024); Wang *et al.* (2024a) or prompts Mahmud *et al.* (2024a); Zhao *et al.* (2024). For example, DG-SCT Duan *et al.* (2024) proposes a dual-guided spatial-channel-temporal attention mechanism to enhance audiovisual feature encoding within transformer layers; AVMoE Cheng *et al.* (2024) employs a mixture-of-experts strategy to dynamically adjust uni-modal and cross-modal adapters. These studies also leverage modality-specific pretrained transformers (*e.g.*, Swin-V2-L Liu *et al.* (2022) for visual and HTS-AT Chen *et al.* (2022b) for audio), leading to improved performance. However, despite these advancements, these PETL-based methods incur significant memory overhead, as training the inserted adapters or prompts requires gradient propagation back through deep transformer layers.

2.3 Memory-Efficient Transfer Learning

Memory-Efficient Transfer Learning (METL) is still in its early stages, with most studies primarily focusing on the vision or NLP domains. Early works aim to reduce training memory through computational optimizations, such as mixed precision Micikevicius *et al.* (2017), quantization strategies Wang *et al.* (2018), or by avoiding activation storage Gomez *et al.* (2017). More recently, LST Sung *et al.* (2022) proposes training a lightweight auxiliary network separate from the pretrained transformer, restricting gradient flow to the smaller network. Other approaches model interactions across transformer layers using lightweight layers Diao *et al.* (2024b) or limit gradient backpropagation to only the final transformer layer Diao *et al.* (2024a). However, these methods primarily focus on METL in the vision-language domain and have not been evaluated on the audiovisual downstream tasks. Moreover, they are not compatible with the pixel-level segmentation task studied in this paper. Technically, our method differs in that it learns and utilizes compact meta-tokens for downstream adaptation and is evaluated on both audiovisual classification and segmentation tasks. Our experiments also indicate that our method achieves a better trade-off between accuracy and efficiency compared to these methods.

3 Method

In this section, we elaborate on the proposed Meta-Token Learning (*Mettle*), a memory-efficient approach for adapting large-scale pretrained transformers to downstream audiovisual tasks. An overview of *Mettle* is illustrated in Figure 2. We first introduce the *Layer-Centric Distillation (LCD)* module, which distills meta-tokens from representations embedded by each pretrained transformer layer. LCD proves effective for audiovisual classification tasks, including AVEL Tian *et al.* (2018b) and AVVP Tian *et al.* (2020). To extend *Mettle* to the pixel-level segmentation task, AVS Zhou *et al.* (2022b), we introduce the *Meta-Token Injection (MTI)* module. Both LCD and MTI are designed with parameter efficiency in mind, making our method both parameter and memory efficient. The following subsections provide a detailed explanation of our method.

3.1 Audio-Visual Tokenization

Given a T -second audible video, we extract an RGB frame and a corresponding 1-second mel-spectrogram at each timestamp. Both modalities are tokenized using a patch-based embedding strategy, where the inputs are divided into non-overlapping patches of fixed size. A linear Dosovitskiy (2021); Liu *et al.* (2022) or

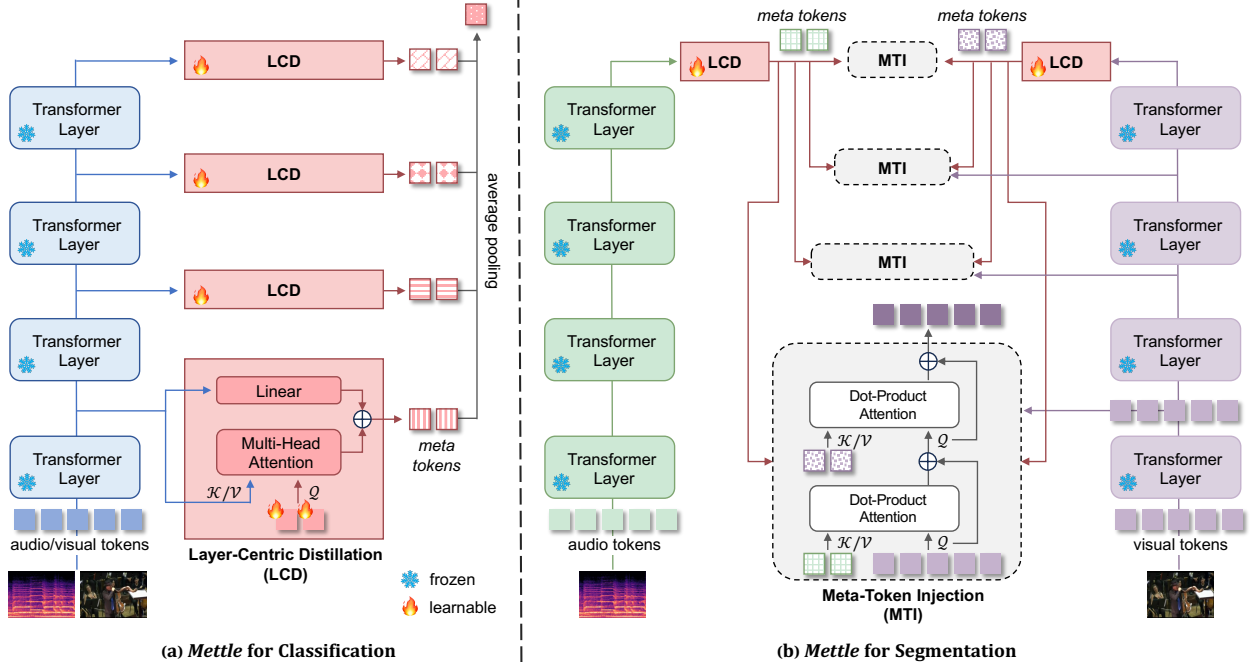


Figure 2. Illustration of our Meta-Token Learning (Mettle) framework. We introduce *Mettle* for both classification tasks, including AVEL Tian et al. (2018b) and AVVP Tian et al. (2020) and the segmentation task, namely AVS Zhou et al. (2022b). (a) For the classification task, we propose the *Layer-Centric Distillation (LCD)* module to distill features from each pretrained transformer layer into learnable meta-tokens. The distilled meta-tokens across transformer layers are further aggregated using simple average pooling for class prediction. LCD is applied at each timestamp for audio and visual modalities. (b) For the segmentation task, LCD is applied only at the final stage of the pretrained transformers to capture high-level semantics. Then, through the *Meta-Token Injection (MTI)* module, the distilled audio and visual meta-tokens are injected into fine-grained visual tokens embedded by earlier transformer layers, better adapting the features for downstream task.

CNN-based Chen et al. (2022b) embedding layer is then applied to obtain initial visual token features $\mathbf{v}_t \in \mathbb{R}^{N_v \times D_v}$ and audio token features $\mathbf{a}_t \in \mathbb{R}^{N_a \times D_a}$, where N_v and N_a denote the number of tokens, and D_v and D_a represent the feature dimensions. These tokenized features are then fed into L -layer pretrained transformers Dosovitskiy (2021); Liu et al. (2022); Chen et al. (2022b) for feature embedding.

3.2 Mettle for Classification

Layer-Centric Distillation (LCD). Studies have shown that pretrained transformer features encode rich information, with different layers capturing distinct patterns Ghiasi et al. (2022); Zhang et al. (2022); Becker et al. (2018). The Layer-Centric Distillation (LCD) module is proposed to extract essential knowledge from each transformer layer, condensing it into *meta-tokens* for downstream tasks. As illustrated in Figure 2a, LCD operates independently for the audio and visual modalities. Next, we describe the LCD process using the visual modality as an example.

Given the visual tokens $\mathbf{v}_t^l \in \mathbb{R}^{N_v^l \times D_v^l}$ from the l -th layer of a pretrained transformer ($l = \{1, 2, \dots, L\}$), the meta-tokens $\mathbf{m}_t^l \in \mathbb{R}^{K \times D_v^l}$ are *task-specific* learnable vectors with the same channel dimension as \mathbf{v}_t^l . These meta-tokens are randomly initialized and refined during later distillation. K is the number of meta-tokens,

which may differ between audio and visual modalities, and $K \ll N_v^l$.

To distill v_t^l into m_t^l , we leverage the multi-head attention Vaswani et al. (2017) mechanism. Specifically, the meta-tokens m_t^l serve as the *query*, while the visual tokens v_t^l act as *key* and *value*, formulated as:

$$m_t^l \leftarrow \text{Softmax} \left((m_t^l \mathbf{W}_Q^l) (v_t^l \mathbf{W}_K^l)^\top \right) (v_t^l \mathbf{W}_V^l), \quad (3.1)$$

where $\mathbf{W}_Q^l, \mathbf{W}_K^l, \mathbf{W}_V^l \in \mathbb{R}^{D_v^l \times D_v^l}$ are learnable parameters. The operator ‘ \leftarrow ’ indicates that the meta-tokens m_t^l are updated. By capturing the interactions between m_t^l and v_t^l through dynamic attention weights, task-relevant representations from v_t^l are effectively distilled into the more compact m_t^l , enhancing their *task-specific* adaptability.

Meanwhile, we introduce a parallel pathway that performs direct token reduction via a linear projection, providing a complementary representation that maintains a more direct relationship with the original *pretrained knowledge*.

Consequently, the final distilled meta-tokens m_t^l are computed as:

$$m_t^l \leftarrow m_t^l + \mathbf{W}_g^l v_t^l, \quad (3.2)$$

where $\mathbf{W}_g^l \in \mathbb{R}^{K \times N_v^l}$ is the learnable parameter of linear layer. This process can be repeated for R iterations, forming an R -step layer-centric distillation.

As shown in Figure 2a, LCD is applied to each pretrained transformer layer, generating layer-wise meta-tokens $m_t^l \in \mathbb{R}^{K \times D_v^l}$ ($l = \{1, \dots, L\}$). In hierarchical transformers such as Swin-V2-L Liu et al. (2022), the channel dimension D_v^l varies across layers. To ensure consistency, an independent linear layer is applied to project each layer’s meta-token dimension to a fixed value d_v . Then, meta-tokens from multiple layers are aggregated into a single meta-token $\bar{m}_t \in \mathbb{R}^{1 \times d_v}$ using parameter-free average pooling, formulated as,

$$\bar{m}_t = \frac{1}{LK} \sum_{l=1}^L \sum_{k=1}^K m_{t,k}^l, \quad (3.3)$$

where $m_{t,k}^l$ is the k -th token of m_t^l ($k = \{1, \dots, K\}$). Such cross-layer aggregation allows the model to comprehensively utilize diverse and useful information embedded in meta-tokens across multiple layers.

By extending the above LCD operations for all T timestamps of visual and audio modalities, we obtain the segment-level visual and audio meta-tokens, denoted as $\bar{v} \in \mathbb{R}^{T \times d_v}$ and $\bar{a} \in \mathbb{R}^{T \times d_a}$, respectively. Then, they can be utilized for downstream audiovisual classification tasks (e.g., AVEL Tian et al. (2018b) and AVVP Tian et al. (2020)) following prior works Duan et al. (2024); Cheng et al. (2024).

3.3 Mettle for Segmentation

For segmentation tasks such as AVS Zhou et al. (2022b), compact meta-tokens alone are insufficient for generating pixel-level segmentation maps, which typically rely on multiple high-resolution visual feature maps encoded by pretrained transformers Duan et al. (2024); Cheng et al. (2024). Therefore, we consider enhancing the multi-resolution visual features using the distilled audio and visual meta-tokens. We explain the details next.

Layer-Centric Distillation (LCD). We apply LCD exclusively to the final layer of the pretrained transformer

for meta-token distillation, as features embedded from the later stages of deep neural networks capture higher-level global semantics Ghiasi et al. (2022) (we will provide more discussions on this design in Sec. 4.4.3). This is particularly relevant in the Swin-V2-L Liu et al. (2022) backbone, where the final stage has a larger receptive field. The meta-token distillation process follows Eqs. 3.1 and 3.2. The distilled audio and visual meta-tokens at the t -th timestamp are denoted as $\mathbf{m}_t^a \in \mathbb{R}^{K_a \times d_a}$ and $\mathbf{m}_t^v \in \mathbb{R}^{K_v \times d_v}$, respectively, where $d_a = d_v$.

Meta-Token Injection (MTI). Unlike the direct aggregation of meta-tokens used in classification tasks, MTI injects knowledge encoded in meta-tokens \mathbf{m}_t^a and \mathbf{m}_t^v into multi-resolution visual features extracted by pretrained transformer layers, adapting them for downstream AVS task, *i.e.*, improving their ability to capture sounding objects.

Specifically, given the visual tokens $\mathbf{v}_t^l \in \mathbb{R}^{N_v^l \times D_v^l}$ extracted by the l -th transformer layer, the audio and visual meta-tokens are first processed by independent linear layers to match the channel dimensions of \mathbf{v}_t^l . Then, MTI consists of two steps: *cross-modal* injection and *intra-modal* injection. As shown in Figure 2b, the aligned audio meta-token $\mathbf{m}_t^a \in \mathbb{R}^{K_a \times D_v^l}$ and visual meta-token $\mathbf{m}_t^v \in \mathbb{R}^{K_v \times D_v^l}$ sequentially interact with the visual tokens \mathbf{v}_t^l . In each injection step, dot-product attention Vaswani et al. (2017) is first used to encode the cross-modal or intra-modal relations between meta-tokens and visual tokens, followed by a residual connection. This process is formulated as follows:

$$\begin{aligned} \mathbf{v}_t^l &\leftarrow \mathbf{v}_t^l + \text{Softmax}\left(\mathbf{v}_t^l (\mathbf{m}_t^a)^\top\right) \mathbf{m}_t^a, \\ \mathbf{v}_t^l &\leftarrow \mathbf{v}_t^l + \text{Softmax}\left(\mathbf{v}_t^l (\mathbf{m}_t^v)^\top\right) \mathbf{m}_t^v. \end{aligned} \tag{3.4}$$

Apart from several preprocessing linear layers, the above injection process is parameter-free, distinguishing it from prior methods that employ complex audio-visual adapters with a large number of learnable parameters Lin et al. (2023); Duan et al. (2024); Cheng et al. (2024); Wang et al. (2024a). Moreover, the MTI is inserted only into the four stages of the pretrained transformer. The updated visual tokens \mathbf{v}_t^l from these stages are sent to an FPN-based decoder Zhou et al. (2022b) in the AVS task to generate segmentation maps.

4 Experiments

4.1 Experimental Setups

Datasets and Metrics. We evaluate our method on three downstream audio-visual learning tasks: Audio-Visual Event Localization (AVEL), Audio-Visual Video Parsing (AVVP), and Audio-Visual Segmentation (AVS). The definitions of these tasks are provided in Sec. 2.1. Here, we briefly introduce the corresponding datasets and evaluation metrics. For the **AVEL** task, we conduct experiments on the AVE Tian et al. (2018b) dataset, which contains 4,143 videos across 28 event categories. Following prior works, we use segment-level accuracy (Acc.) to evaluate predicted audio-visual events. For the **AVVP** task, we use the LLP Tian et al. (2020) dataset, which consists of 11,849 videos spanning 25 categories. Following Tian et al. (2020), we report the F1-score of predicted audio events, visual events, and audio-visual events at both segment-level and event-level. For the **AVS** task, we evaluate both single-source and multi-source segmentation using the S4 and MS3 subsets of AVSBench Zhou et al. (2022b). These subsets contain 4,932 and 404 videos, respectively, covering 23 classes. We use mean Intersection over Union (mIoU) as the evaluation metric.

Table 1. Comparison on audio-visual event localization task. We evaluate our model using both modality-shared and modality-separate transformer backbones. In various setups, our method has competitive accuracy while significantly reducing memory and runtime costs.

Method	Visual Encoder	Audio Encoder	Visual Pretrain Dataset	Audio Pretrain Dataset	Trainable Params (%) ↓	Total Params (M) ↓	Memory (GB) ↓	Runtime (ms) ↓	Acc ↑
AVEL Tian et al. (2018b)	ResNet-152	VGGish	ImageNet	AudioSet	2.7	136.0	N/A	N/A	74.0
AVSDN Lin et al. (2019)	ResNet-152	VGGish	ImageNet	AudioSet	5.7	140.3	N/A	N/A	75.4
CMRAN Xu et al. (2020)	ResNet-152	VGGish	ImageNet	AudioSet	10.7	148.2	N/A	N/A	78.3
MM-Pyramid Yu et al. (2022)	ResNet-152	VGGish	ImageNet	AudioSet	25.0	176.3	N/A	N/A	77.8
CMBS Xia & Zhao (2022)	ResNet-152	VGGish	ImageNet	AudioSet	6.6	216.7	N/A	N/A	79.7
LAVisH Lin et al. (2023)	ViT-L-16 (shared)		ImageNet	✗	4.3	340.1	19.2	328.3	78.1
CoPL Zhao et al. (2024)	ViT-L-16 (shared)		ImageNet	✗	1.5	332.8	N/A	N/A	79.2
AVMoE Cheng et al. (2024)	ViT-L-16 (shared)		ImageNet	✗	32.6	483.1	19.5	461.5	79.2
MA-AVT Mahmud et al. (2024a)	ViT-L-16 (shared)		ImageNet	✗	3.7	338.4	7.2	448.5	79.6
<i>Mettle (ours)</i>	ViT-L-16 (shared)		ImageNet	✗	38.8	532.2	1.7	146.2	80.6
LAVisH Lin et al. (2023)	Swin-V2-L (shared)		ImageNet	✗	2.7	238.8	15.4	322.1	81.1
AVMoE Cheng et al. (2024)	Swin-V2-L (shared)		ImageNet	✗	39.4	374.4	16.8	500.0	81.5
STG-CMA Wang et al. (2024a)	Swin-V2-L (shared)		ImageNet	✗	8.9	214.0	5.9	429.5	82.5
<i>Mettle (ours)</i>	Swin-V2-L (shared)		ImageNet	✗	37.2	364.4	1.8	125.4	82.3
LAVisH Lin et al. (2023)	Swin-V2-L	HTS-AT	ImageNet	AudioSet	30.6	374.9	11.9	232.9	78.6
DG-SCT Duan et al. (2024)	Swin-V2-L	HTS-AT	ImageNet	AudioSet	43.6	461.3	13.1	316.7	82.2
AVMoE Cheng et al. (2024)	Swin-V2-L	HTS-AT	ImageNet	AudioSet	34.9	404.0	12.1	256.1	82.6
<i>Mettle (ours)</i>	Swin-V2-L	HTS-AT	ImageNet	AudioSet	23.0	338.0	1.5	88.3	83.3

Implementation Details. We train and evaluate our model using various large-scale pretrained transformer backbones, including ViT-L-16 Xu et al. (2022), Swin-V2-L Liu et al. (2022), and HTS-AT Chen et al. (2022b). In some experiments, following prior work LAVisH Lin et al. (2023), we use ViT-L-16 or Swin-V2-L for both audio and visual modalities (*shared*) to show that a model pretrained only in the vision domain can be adapted to audiovisual domain. As illustrated in Figure 2, our *Mettle* approach serves as the early audio and visual encoder. Task-specific decoders are then applied to generate predictions following Duan et al. (2024); Cheng et al. (2024). Additional details on batch size, learning rate, training epochs, and other training hyper-parameters for different tasks are provided in Sec. A of our Appendix. All of our experiments are conducted on an NVIDIA A100-SXM4-40GB GPU.

4.2 Main Results

In this section, we present quantitative comparisons of our *Mettle* method against prior approaches on downstream audiovisual tasks, with a particular focus on recent parameter-efficient tuning methods, *e.g.*, LAVisH Lin et al. (2023), DG-SCT Duan et al. (2024), and AVMoE Cheng et al. (2024). For each task, in addition to the task-specific evaluation metrics introduced in Sec. 4.1, we report the proportion of trainable parameters (%) and the total number of parameters (M) to assess parameter efficiency. Additionally, we measure training memory usage (GB) and runtime (ms)¹ to evaluate memory efficiency. Notably, these two metrics, ignored by prior works, are recorded during the model training process and normalized by batch size.

4.2.1 Results on Audio-Visual Event Localization

Table 1 presents the comparison results. We evaluate our method using various transformer backbones, including modality-shared ViT-L-16 Dosovitskiy (2021) and Swin-V2-L Liu et al. (2022), as well as modality-separate Swin-V2-L (visual) and HTS-AT Chen et al. (2022b) (audio). As shown in the Table, our method achieves comparable or superior accuracy compared to prior methods. Notably, our approach remains

¹We do not adopt the training GPU hours as the metric, as it is hard to fairly determine the optimal convergence points of prior methods during our reproduction. But, the GPU hours are expected to follow similar trends as the runtime.

Table 2. Comparison on the audio-visual video parsing task. ‘Avg.’ is the average value of segment-level and event-level metrics. Swin-V2-L Liu et al. (2022) and HTS-AT Chen et al. (2022b) are used as the visual and audio transformer backbones, respectively.

Method	Trainable Params (%) ↓	Total Params (M) ↓	Memory (GB) ↓	Runtime (ms) ↓	Segment-level ↑					Event-level ↑					Avg. ↑
					A	V	AV	Type	Event	A	V	AV	Type	Event	
HAN Tian et al. (2020)	N/A	N/A	N/A	N/A	60.1	52.9	48.9	54.0	55.4	51.3	48.9	43.0	47.7	48.0	51.0
MGN Mo & Tian (2022)	N/A	N/A	N/A	N/A	60.7	55.5	50.6	55.6	57.2	51.0	52.4	44.4	49.3	49.2	52.6
DG-SCT Duan et al. (2024)	43.3	458.9	8.5	299.3	59.0	59.4	52.8	57.1	57.0	49.2	56.1	46.1	50.5	49.1	53.6
AVMoE Cheng et al. (2024)	30.9	376.4	12.9	490.0	62.1	60.0	54.4	58.8	59.0	51.8	55.7	47.6	51.7	50.2	55.1
<i>Mettle (ours)</i>	8.3	283.5	0.6	64.2	64.3	55.9	50.9	57.0	61.2	56.1	52.2	45.1	51.1	53.1	54.7

Table 3. Comparison on the audio-visual segmentation task. We evaluate our approach on both the single-source (S4) and multi-source (MS3) segmentation problems.

Method	Visual Encoder	Audio Encoder	Visual Pretrain Dataset	Audio Pretrain Dataset	Trainable Params (%) ↓	Total Params (M) ↓	Memory (GB) ↓	Runtime (ms) ↓	S4 (mIoU) ↑	MS3 (mIoU) ↑
AVS Zhou et al. (2022b)	PVT-V2	VGGish	ImageNet	AudioSet	58.7	174.5	4.8	647.0	78.7	54.0
LAViSH Lin et al. (2023)	Swin-V2-L (shared)		ImageNet	×	14.0	266.4	5.9	222.6	80.1	49.8
<i>Mettle (ours)</i>	Swin-V2-L (shared)		ImageNet	×	11.1	257.2	2.7	113.2	79.9	53.7
DG-SCT Duan et al. (2024)	Swin-V2-L	HTS-AT	ImageNet	AudioSet	61.5	594.8	9.0	330.3	80.9	53.5
AVMoE Cheng et al. (2024)	Swin-V2-L	HTS-AT	ImageNet	AudioSet	54.4	501.2	9.5	427.3	81.1	54.5
<i>Mettle (ours)</i>	Swin-V2-L	HTS-AT	ImageNet	AudioSet	21.6	291.7	2.9	105.7	80.7	55.1

effective even with modality-shared ViT-L-16 and Swin-V2-L backbones, demonstrating that the vision-domain knowledge can be memory-efficiently adapted to downstream audiovisual tasks. This also highlights the generalization capability of our method. The last row of Table 1 shows that our method achieves the highest performance when using modality-separate backbones. This is expected, as HTS-AT is pretrained on an audio-domain dataset AudioSet Gemmeke et al. (2017), enabling it to encode more effective audio representations, thereby improving meta-token distillation. More importantly, our approach achieves competitive accuracy with significantly lower parameters and memory costs. For instance, compared to the state-of-the-art method AVMoE Cheng et al. (2024), our model reduces the total parameter count by 66M and decreases the proportion of learnable parameters by 11.9%. Moreover, AVMoE requires 12.1GB of memory per sample and 256.1ms per iteration during training. In contrast, our model requires only 1.5GB and takes 88.3ms, demonstrating superior efficiency.

4.2.2 Results on Audio-Visual Video Parsing

We compare our method with prior models on the audio-visual video parsing task. For a fair comparison with prior works Duan et al. (2024); Cheng et al. (2024), we adopt Swin-V2-L Liu et al. (2022) and HTS-AT Chen et al. (2022b) as the visual and audio transformer backbones, respectively. As shown in Table 2, our method outperforms DG-SCT Duan et al. (2024) by 1.1% in the average metric (‘Avg.’) and achieves competitive performance with the state-of-the-art AVMoE Cheng et al. (2024). We observe an imbalance between audio prediction (‘A’) and visual prediction (‘V’) metrics. This discrepancy arises from the inherent challenges of the AVVP task, where only weak video-level labels are available, and the modality-specific event labels are unknown. To ensure a fair comparison with recent parameter-efficient methods, we do not utilize additional video-level or segment-level pseudo labels proposed in recent studies Wu & Yang (2021); Cheng et al. (2022); Lai et al. (2023). Despite this constraint, our method maintains competitive accuracy under the same conditions while demonstrating superior parameter and memory efficiency. Compared to AVMoE Cheng et al. (2024), our *Mettle* significantly reduces the trainable parameters (30.9% → 8.3%) and total parameters (376.4M → 283.5M). Moreover, our model dramatically lowers memory consumption (12.9GB → 0.6GB) and training runtime (490.0ms → 64.2ms).

Table 4. Comparison with state-of-the-art memory-efficient methods from vision-language field. Our method consistently outperforms them in accuracy on both tasks, demonstrating a better trade-off between accuracy and efficiency.

Method	Venue	AVEL				AVVP			
		Total Params (M) ↓	Memory (GB) ↓	Runtime (ms) ↓	Acc. ↑	Total Params (M) ↓	Memory (GB) ↓	Runtime (ms) ↓	Avg. ↑
LST Sung et al. (2022)	NeurIPS'22	347.8	1.3	79.0	80.0	286.1	0.6	59.0	51.9
UniPT Diao et al. (2024b)	CVPR'24	343.2	1.3	83.9	81.1	285.5	0.6	61.2	52.4
SHERL Diao et al. (2024a)	ECCV'24	347.7	1.0	90.7	81.6	286.0	0.6	71.7	52.1
<i>Mettle (ours)</i>	-	338.0	1.5	88.3	83.3	283.5	0.6	64.2	54.7

4.2.3 Results on Audio-Visual Segmentation

Table 3 shows the comparison results for the pixel-level AVS task. Our method demonstrates superior accuracy, as well as improved parameter and memory efficiency. When using the modality-shared Swin-V2-L backbone, our approach attains comparable mIoU to LAVisH [Lin et al. \(2023\)](#) in the single-source S4 setting and significantly outperforms it by 3.9% mIoU in the multi-source MS3 setting. Furthermore, our model requires fewer parameters and consumes only half the training memory and runtime of LAVisH. The efficiency gains become even more pronounced when employing modality-separate backbones. As shown in the lower part of Table 3, compared to prior method AVMoE [Cheng et al. \(2024\)](#), our method achieves comparable mIoU in the S4 setting and surpasses prior work in the MS3 setting, while reducing trainable parameter count by 77%, memory by 69%, and runtime by 75%.

4.3 Further Comparisons

In Sec. 4.2, we presented extensive experiments comparing our method with existing parameter-efficient audiovisual fine-tuning methods [Lin et al. \(2023\)](#); [Duan et al. \(2024\)](#); [Cheng et al. \(2024\)](#), demonstrating its superiority in parameter efficiency, memory usage, and training time while maintaining competitive performance. In this section, we provide additional comparisons with several representative memory-efficient methods from the vision-language domain, as well as two variant baseline approaches. The details are described below.

4.3.1 Comparison with Memory-efficient Methods from the Vision-language field

Current exploration of the memory-efficient methods primarily focus on the vision-language domain, while our work represents the first attempt in the audiovisual field. For a comprehensive comparison, we try to adapt several state-of-the-art memory-efficient methods from the vision-language domain – LST [Sung et al. \(2022\)](#), UniPT [Diao et al. \(2024b\)](#), and SHERL [Diao et al. \(2024a\)](#), to the studied audiovisual downstream tasks. As these methods are not applicable to pixel-level segmentation, we focus our comparisons on the AVEL and AVVP classification tasks. As shown in Table 4, our method uses fewer parameters, and achieves comparable training memory usage and runtime compared with these meticulously designed baselines. Moreover, our method consistently outperforms them in accuracy on both tasks, demonstrating a better trade-off between accuracy and efficiency.

4.3.2 Comparison with two vanilla Audiovisual Approaches

We also compare our method with two vanilla approaches: 1) *Direct Connection*. Audio and visual features extracted by the pretrained transformer backbones are directly used for downstream tasks. 2) *Linear Probing*. A modality-independent linear layer is added to the final layer of the pretrained transformer backbone for

Table 5. Comparison with two vanilla approaches. ‘Direct’ refers to using features extracted by frozen transformer models directly for downstream tasks. ‘Linear’ represents the linear probing strategy, where a modality-separate linear layer is added after the final frozen transformer layer.

Method	AVEL	AVVP					AVS	
	Acc.	Segment-level Type	Event	Event-level Type	Event	Avg.	S4 mIoU	MS3 mIoU
Direct	80.7	55.3	57.0	49.0	49.1	52.3	78.8	48.7
Linear	78.8	54.8	57.1	48.3	49.5	51.9	79.2	51.8
Ours	82.3	57.0	61.2	51.1	53.1	54.7	79.9	53.7

Table 6. Effect of the number of meta tokens K . We analyze how varying the number of audio (K_a) and visual (K_v) meta tokens affects performance.

K_a	K_v	AVEL	AVVP					AVS	
		Acc.	Segment-level Type	Event	Event-level Type	Event	Avg.	S4 mIoU	MS3 mIoU
1	1	82.3	57.0	61.2	51.1	53.1	54.7	79.9	53.7
1	2	81.2	57.0	62.0	50.6	52.8	54.5	79.6	52.7
2	1	81.2	56.6	60.7	50.4	52.3	54.1	79.4	52.0
2	2	80.7	56.5	60.6	50.3	52.1	54.0	79.7	52.6
4	4	80.8	56.1	60.4	49.7	51.9	53.6	79.8	52.3

task-specific adaptation. Notably, for the AVS [Zhou et al. \(2022b\)](#) task, the features updated by linear probing are further processed by our proposed meta-token injection (MTI) modules. [Table 5](#) presents the comparison results. Compared to the *Direct Connection* approach, although the *Linear Probing* strategy introduces learnable layers, it does not improve performance on the AVEL and AVVP tasks but proves beneficial for AVS when combined with our MTI module. Nevertheless, our method, which uses layer-centric distillation and meta-token injection, significantly outperforms both approaches.

4.4 Ablation Studies

In this section, we conduct ablation studies to analyze the effects of key hyper-parameters and the core components of our Layer-Centric Distillation (**LCD**) and Meta-Token Injection (**MTI**) modules. For simplicity, we primarily report the accuracy-based metrics in the ablations. Unless otherwise specified, we use a modality-shared Swin-V2-L [Liu et al. \(2022\)](#) backbone for the AVEL and AVS tasks. For the AVVP task, modality-specific backbones are adopted, with Swin-V2-L for the visual modality and HTS-AT [Chen et al. \(2022b\)](#) for the audio modality.

4.4.1 Hyperparameter Studies

Effect of the Meta-Token Number K . In the LCD module, we introduce K learnable meta-tokens distilled from pretrained transformer layers. The numbers may be different for audio and visual modalities, denoted as K_a and K_v , respectively. [Table 6](#) presents the ablation results. For most downstream audiovisual tasks, using a single meta-token per modality seems sufficient to achieve high performance. This design ensures that the learned meta-token remains highly compact for downstream adaptation while minimizing redundancy in features encoded by pretrained backbones. To provide a more in-depth analysis, in [Figure 3](#), we plot the loss landscapes of models trained with different numbers of meta tokens ($K = \{1, 4\}$), evaluated on the AVEL task. The comparison reveals that using a larger number of meta tokens results in a more rugged optimization landscape with multiple local minima, which may hinder convergence. In contrast, fewer meta tokens

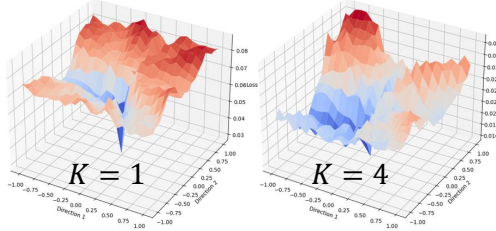


Figure 3. Loss landscape of models trained with different numbers of meta-tokens. The subfigures are generated using models with a modality-shared Swin-V2-L backbone, evaluated on the AVEL task.

Table 7. Effect of using hierarchical meta-token numbers. Swin-V2-L Liu et al. (2022) and HTS-AT Chen et al. (2022b), both featuring hierarchical designs, are used as the visual and audio backbones, respectively. Each backbone consists of four-stage transformer layers. The first column presents different choices for the meta-token numbers at four stages (e.g., the {8,4,2,1} indicates that the layers in the first bottom stage use 8 meta-tokens while layers of the fourth top stage use 1 meta-token). The ‘default’ setting denotes that all transformer stages/layers share the same meta-token numbers.

Setup	AVEL	AVVP				Avg.
	Acc.	Segment-level Type	Event	Type	Event	
{8,4,2,1}	80.7	55.3	57.0	49.0	49.1	52.3
{2,2,1,1}	78.8	54.8	57.1	48.3	49.5	51.9
default	82.3	57.0	61.2	51.1	53.1	54.7

lead to a smoother landscape, potentially making the model easier to optimize and improving performance. The optimal token number may differ slightly when using the modality-separate backbones (Swin-V2-L & HTS-AT) for AVEL and AVS tasks. For example, in this setup, the model has the best performance with one audio meta-token and two visual meta-tokens (still quiet few) for the AVEL task. The final choice of meta-token numbers is provided in Sec. A of our Appendix.

Effect of using Hierarchical Design for Meta-Tokens. In our LCD module, the audio/visual meta-token numbers K remain identical across different transformer layers (i.e., $K_a = K_v = K$). For transformers with hierarchical designs, e.g., Swin-V2-L Liu et al. (2022) and HTS-AT Chen et al. (2022b), earlier layers encode more audio/visual tokens, while the later (top) layers contain fewer tokens. A natural question arises: what if we also adopt a hierarchical number of meta-tokens in the layer-centric distillation process? To explore this, we test two designs. Both Swin-V2-L and HTS-AT consist of four transformer stages. First, based on prior experimental results, we set the meta-token number at the last stage to 1. In our first design, we define the meta-token numbers using a factor of 2. As a result, the first (bottom) stage uses 8 meta-tokens, the second stage uses 4 meta-tokens, and the third stage uses 2, denoted as ‘{8,4,2,1}’ in Table 7. In our second design, the top two stages use 1 meta-token each, while the bottom two stages use 2 meta-tokens each, resulting in ‘{2,2,1,1}’ in Table 7. As shown in the Table, neither hierarchical design improves the model’s performance, indicating that hierarchical meta-token numbers are unnecessary for distillation. Consequently, we choose to use identical meta-tokens across all transformer layers/stages. This also simplifies the implementation and further reduces the number of learnable parameters.

Effect of the Distillation Step R . The distillation process operates through R -step cycles (Eq. 3.2), iteratively updating the meta-tokens. We denote the distillation steps for audio and visual modalities as R_a and R_v , respectively. Table 8 presents the ablation results. A single-step distillation per modality has guaranteed high

Table 8. Effect of the number of distillation steps R . We study the impact of varying the number of audio (R_a) and visual (R_v) distillation iterations.

R_a	R_v	AVEL	AVVP					AVS	
		Acc.	Segment-level Type	Event	Event-level Type	Event	Avg.	S4 mIoU	MS3 mIoU
1	1	82.3	57.0	61.2	51.1	53.1	54.7	79.6	53.7
1	2	80.9	55.8	60.9	49.5	52.0	53.4	79.9	53.5
2	1	80.7	56.7	61.2	50.4	52.5	54.2	79.9	53.7
2	2	81.1	56.4	60.6	50.0	51.9	53.8	79.8	53.2
4	4	81.6	56.6	61.1	50.3	52.6	54.1	79.8	52.3

Table 9. Component ablation of LCD. ‘TS’ represents the Task-Specific meta-token tuning branch, and ‘DP’ denotes the linear branch for preserving Domain-Pretrained knowledge.

Component		AVEL	AVVP					AVS	
TS	DP	Acc.	Segment-level Type	Event	Event-level Type	Event	Avg.	S4 mIoU	MS3 mIoU
×	✓	77.3	55.3	60.1	49.0	51.8	52.9	78.9	52.7
✓	×	80.5	56.2	60.8	49.7	51.6	53.6	78.6	51.5
✓	✓	82.3	57.0	61.2	51.1	53.1	54.7	79.9	53.7

performances for most downstream tasks. This design choice keeps our model lightweight, reducing the number of learnable parameters and computational overhead. By analyzing Table 6 and Table 8, we observe that classification tasks such as AVEL and AVVP are more sensitive to distillation-related hyperparameters. This is reasonable since these tasks heavily rely on distilled meta-tokens for final classification. In contrast, for the segmentation task, visual feature maps embedded by pretrained transformers play a more critical role in determining final segmentation results.

4.4.2 Ablation Studies on LCD

Component Ablation of LCD. The LCD module comprises two key components: 1) The learnable meta-tokens are introduced to interact with pretrained features for Task-Specific adaptation (Eq. 3.1); 2) A lightweight linear layer is used to better retain Domain-Pretrained knowledge (Eq. 3.2). We denote these components as **TS** and **DP**, respectively. The ablation results are shown in Table 9. Removing either component leads to a significant performance drop across all downstream audio-visual tasks. For example, in the AVEL task, excluding the TS component reduces accuracy from 82.3% to 77.3%. These results highlight the necessity of both pretrained knowledge preservation and task-specific adaptation in the LCD module.

Linear layer vs. Average Pooling in LCD. Our LCD module incorporates a linear layer branch to process the original audio or visual tokens embedded by the pretrained transformer model, complementing the branch that utilizes meta-tokens. We also explore a parameter-free variant that replaces the linear layer with direct average pooling on the original audio/visual token features. As shown in Table 10, compared to removing the branch (‘Remove’), this simple strategy (‘AvgPool.’) also benefits the AVEL and AVS tasks, highlighting the importance of designing a branch to preserve pretrained knowledge. Moreover, the average pooling strategy can achieve comparable performance to the learnable linear layer in AVEL and single-source S4 setting of AVS tasks. The video data in these tasks typically contains a single event or sounding source, making simple average pooling effective. However, for more complex tasks (*i.e.*, the AVVP and AVS-MS3), which involve multiple events, the linear layer proves more effective for LCD.

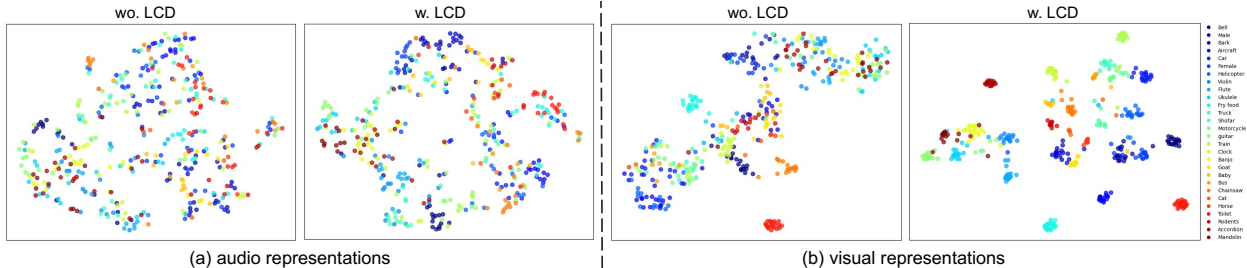


Figure 4. T-SNE visualization of audio and visual meta-token representations. Samples are taken from the test set of the AVE Tian et al. (2018b) dataset.

Table 10. Replacing the linear layer branch of the LCD module with simple average pooling (‘AvgPool.’). The item ‘Remove’ denotes that this branch is completely removed. Swin-V2-L Liu et al. (2022) and HTS-AT Chen et al. (2022b) are used as the visual and audio transformer backbones, respectively.

Strategy	AVEL	AVVP				AVS		
	Acc.	Segment-level Type	Event	Event-level Type	Event	Avg.	S4 mIoU	MS3 mIoU
Remove	80.5	56.2	60.8	49.7	51.6	53.6	78.6	51.5
AvgPool.	83.2	56.4	59.8	49.4	50.4	53.3	80.4	53.8
Linear	83.3	57.0	61.2	51.1	53.1	54.7	80.7	55.1

4.4.3 Ablation Studies on MTI

Component Ablation of MTI. The MTI module is designed for the segmentation AVS task, incorporating both cross-modal and intra-modal injection by utilizing meta-tokens from audio and visual modalities. We ablate their impacts in Table 11. Removing either intra-modal or cross-modal injection degrades the model’s performance to varying degrees, with a more pronounced impact in the more challenging MS3 setting. For example, the mIoU significantly drops by 3.8% without using the cross-modal injection. The MS3 setting involves multiple sound sources, making the guidance from audio meta-tokens crucial for accurately identifying the corresponding sounding objects.

Injection order in MTI module. Our MTI module first applies cross-modal injection followed by intra-modal injection (‘cross-first’). We explore the impact of reversing this order, *i.e.*, the intra-modal injection first. In this setup, the mIoU for the S4 and MS3 settings of the AVS task is 79.8% and 53.3%, respectively, which is very close to the ‘cross-first’ setup (79.9% and 53.7%). This suggests that the injection order has minimal impact on the model’s performance.

Placement of the MTI Module. As shown in Figure 2b, the MTI module is applied by default to combine with the LCD-distilled meta tokens extracted from the last (top) pretrained transformer layer. This design is based on the hypothesis that meta tokens from higher layers contain more accurate and comprehensive global category semantics. To validate this, we conduct experiments on the AVEL classification task by applying LCD to individual transformer layers (1st to 4th). The resulting accuracies are 49.5%, 64.7%, 80.4%, and 81.7%, respectively. This trend suggests that top-layer features indeed capture richer category-level semantics, justifying their use for guiding the MTI module. Furthermore, we apply LCD to both the final and earlier layers and feed the resulting meta tokens into the MTI module. As shown in Table 12, MTI benefits more from high-layer LCD, particularly in the more challenging MS3 setting.

Table 11: Component ablation of MTI. MTI module involves the intra- and cross-modality interactions.

Component		AVS	
intra	cross	S4	MS3
✓	✗	79.3	49.9
✗	✓	79.4	52.3
✓	✓	79.9	53.7

Table 12. Effect of MTI module placement along the transformer depth. Experiments are conducted on the AVS task, and the mIoU metric is reported.

layer index	1st (bottom)	2nd	3rd	4th (top)
S4	80.2	80.3	80.5	80.7
MS3	53.6	53.8	54.5	55.1

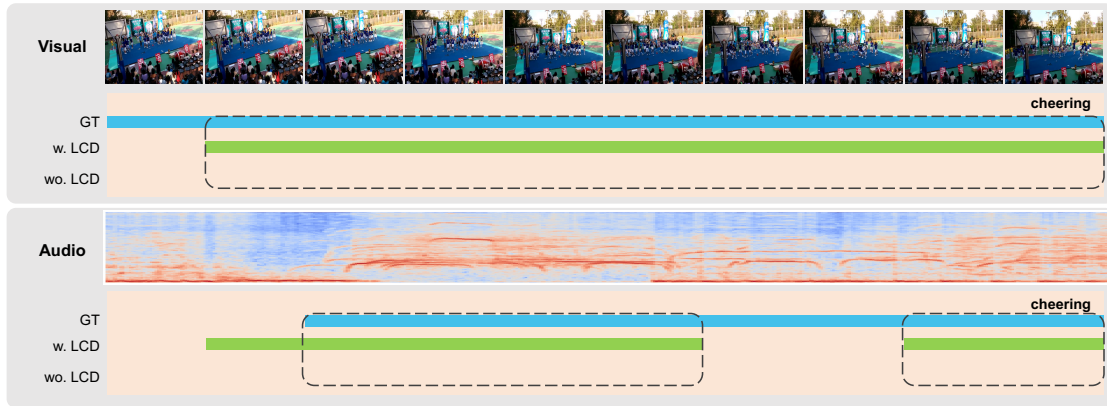
4.5 Qualitative Results

The effectiveness of our approach primarily stems from the layer-centric distillation (LCD), which generates compact meta-tokens to facilitate downstream task adaptation. We provide qualitative results to demonstrate its advantages. Based on the AVEL task, we visualize the representations of learned audio and visual meta-token representations (‘w. LCD’) and compare them to features produced by the frozen pretrained backbone (‘wo. LCD’). The Swin-V2-L is used as shared backbone. As shown in Figure 4, the distilled meta-tokens exhibit better intra-class compactness and inter-class separation for both modalities. These results further validate the effectiveness of our meta-token distillation process: the meta-tokens adapts better to downstream task. We also present some qualitative results on the AVVP and AVS tasks. As shown in Figure 5, our model trained with the layer-centric distillation (‘w. LCD’) more precisely localizes the temporal segments of events, highlighted by the dashed line box. In Figure 6, it better delineates the shape of sounding objects and reduces the over-segmentation of unrelated pixels.

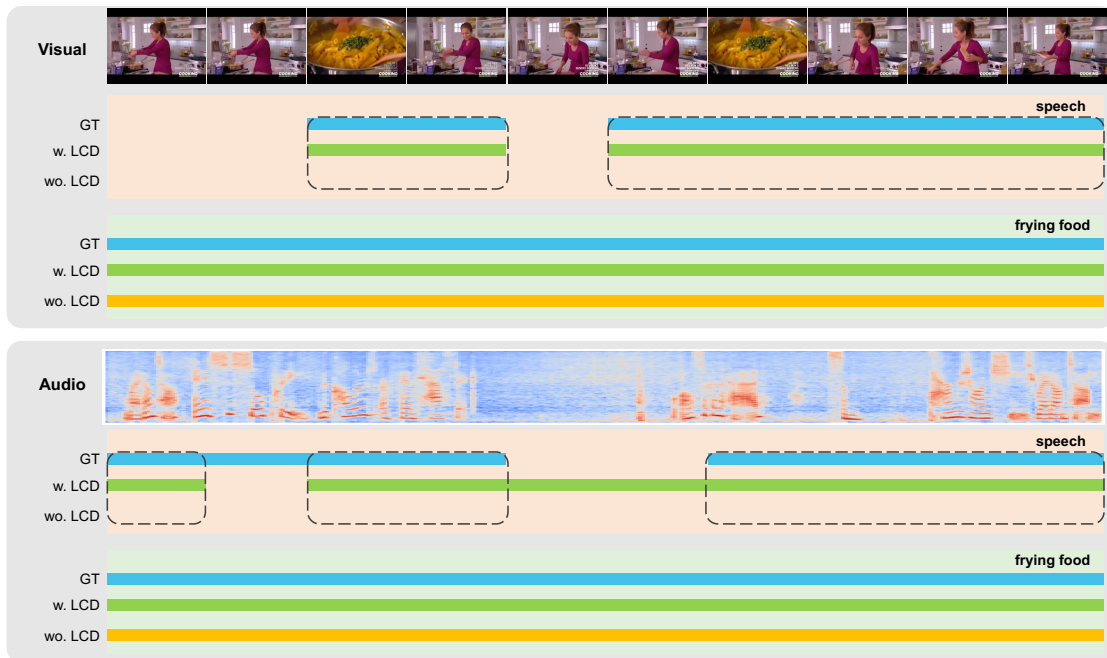
5 Conclusion and Future Work

We found that prior parameter-efficient audio-visual adaptation methods, designed to adapt large-scale pretrained transformers to downstream tasks, exhibit significant memory inefficiency. Our *Mettle* approach mitigates this issue by distilling audio and visual meta-tokens from pretrained backbones in parallel. Specifically, we introduce lightweight layer-centric distillation and meta-token injection modules. The former module performs layer-wise distillation of audio and visual tokens from pretrained transformers into compact meta-tokens, while the latter injects the extracted top-layer meta-tokens into high-resolution audio and visual tokens from earlier layers. Evaluated on three audiovisual classification and segmentation tasks, including AVEL, AVVP, and AVS, our method excels in accuracy, parameter efficiency, memory usage, and training speed, achieving a favorable trade-off among these factors. We will release the source code to the community and hope to inspire further progress in memory-efficient audio-visual adaptation.

Limitation. Despite its effectiveness, our method faces challenges in more complex *reasoning* tasks like audiovisual question answering Li et al. (2022), which involves diverse question types (e.g., *location*, *counting*, and *comparative*) within long, dynamic audio-visual scenarios. Effectively distilling compact meta-tokens that generalize across various questions remains difficult relying solely on frozen intermediate features. To overcome this, our future work will explore integrating memory-efficient modules with partial layer fine-tuning to enhance adaptability to more complex tasks.



(a)



(b)

Figure 5. Qualitative results for the AVVP task. The model trained with the LCD module provides more accurate audio and visual event parsing along the timeline.

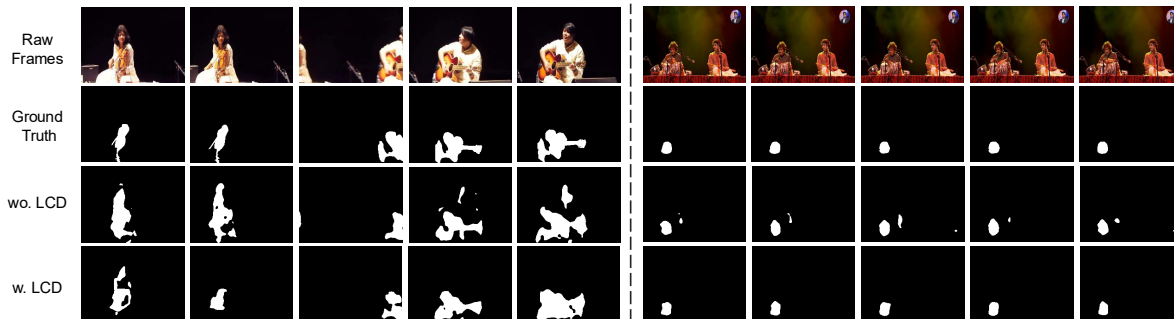


Figure 6. Qualitative results for the AVS task. The model trained with the LCD module generates more accurate segmentation boundaries of the sounding objects.

Appendix

A Training hyperparameters

Table 13 presents the hyperparameter details for training our model on downstream audiovisual learning tasks, including audio-visual event localization (AVEL) Tian et al. (2018b), audio-visual video parsing (AVVP) Tian et al. (2020), and audio-visual segmentation (AVS) Zhou et al. (2022b). We use the same training configurations as shown in Table 13 to train our model with both the modality-shared (Swin-V2-L Liu et al. (2022)) and modality-specific (Swin-V2-L for visual, HTS-AT Chen et al. (2022b) for audio) transformer backbones. For the AVEL and AVS tasks, our ablation studies on hyperparameters related to the layer-centric distillation process (*i.e.*, the meta token number and distillation step) presented in Sec. 4.4 are based on the model trained with modality-shared Swin-V2-L backbone. The best hyperparameters for using modality-specific backbones are provided in Table 14. We will release the source code to facilitate reproducibility and support further advancements in memory-efficient audiovisual adaptation.

Table 13: Training hyperparameters for audiovisual downstream tasks

Hyperparameters	AVEL	AVVP	AVS-S4	AVS-MS3
batch size	16	16	4	4
epochs	10	15	40	30
optimizer	Adam	Adam	Adam	Adam
base learning rate	4e-4	3e-4	1e-4	1e-4
learning rate scheduler	StepLR	StepLR	StepLR	None
↪ step size	3	5	5	N/A
↪ gamma	0.35	0.5	0.8	N/A

Table 14. Hyperparameter details when using modality-specific (Swin-V2-L Liu et al. (2022) for visual, HTS-AT Chen et al. (2022b) for audio) transformer backbones for model training.

Tasks	Meta-token number K		Distillation step R	
	K_a	K_v	R_a	R_v
AVEL	1	2	1	1
AVVP	1	1	1	1
AVS (S4)	1	1	1	2
AVS (MS3)	1	1	1	1

B Extending the Method to CNN Backbone

As demonstrated in the main paper, our method supports hierarchical backbones such as Swin-V2-L Liu et al. (2022), and can therefore be extended to CNN-based backbones as well. In Table 15, we report results using ResNeXt101 Xie et al. (2017) on the AVEL classification and AVS-MS3 segmentation tasks.

Table 15: Results of the model using the ResNeXt101 CNN backbone.

AVEL (classification)				AVS-MS3 (segmentation)			
Param. (M)	Mem. (G)	Time (ms).	Acc.	Param. (M)	Mem. (G)	Time (ms).	mIoU
151.6	1.0	41.8	80.1	151.9	3.7	86.7	48.4

Table 16: Inference runtime comparison.

Methods	AVEL	AVVP	AVS
DG-SCT Duan et al. (2024)	253.2	162.8	240.7
AVMoE Cheng et al. (2024)	140.5	287.5	191.6
Ours	84.4	60.2	73.7

C Inference runtime comparison

In the main paper, we compare the *training*-time runtime of our method with prior audio-visual efficient tuning methods. Here, we additionally provide a comparison of *inference*-time runtime. The results are shown in Table 16. Compared to prior methods, our model consistently achieves significantly lower inference runtime across three audiovisual learning tasks.

References

- Relja Arandjelovic and Andrew Zisserman. Objects that sound. In *ECCV*, pp. 435–451, 2018.
- Ankur Bapna, Naveen Arivazhagan, and Orhan Firat. Simple, scalable adaptation for neural machine translation. *arXiv preprint arXiv:1909.08478*, 2019.
- Sören Becker, Marcel Ackermann, Sebastian Lapuschkin, Klaus-Robert Müller, and Wojciech Samek. Interpreting and explaining deep neural networks for classification of audio signals. *arXiv preprint arXiv:1807.03418*, 2018.
- Guangyi Chen, Weiran Yao, Xiangchen Song, Xinyue Li, Yongming Rao, and Kun Zhang. Plot: Prompt learning with optimal transport for vision-language models. *arXiv preprint arXiv:2210.01253*, 2022a.
- Honglie Chen, Weidi Xie, Triantafyllos Afouras, Arsha Nagrani, Andrea Vedaldi, and Andrew Zisserman. Localizing visual sounds the hard way. In *CVPR*, pp. 16867–16876, 2021.
- Ke Chen, Xingjian Du, Bilei Zhu, Zejun Ma, Taylor Berg-Kirkpatrick, and Shlomo Dubnov. Hts-at: A hierarchical token-semantic audio transformer for sound classification and detection. In *ICASSP*, pp. 646–650, 2022b.
- Yuanhong Chen, Yuyuan Liu, Hu Wang, Fengbei Liu, Chong Wang, Helen Frazer, and Gustavo Carneiro. Unraveling instance associations: A closer look for audio-visual segmentation. In *CVPR*, pp. 26497–26507, 2024.
- Haoyue Cheng, Zhaoyang Liu, Hang Zhou, Chen Qian, Wayne Wu, and Limin Wang. Joint-modal label denoising for weakly-supervised audio-visual video parsing. In *ECCV*, pp. 431–448, 2022.
- Ying Cheng, Ruize Wang, Zhihao Pan, Rui Feng, and Yuejie Zhang. Look, listen, and attend: Co-attention network for self-supervised audio-visual representation learning. In *ACM MM*, pp. 3884–3892, 2020.
- Ying Cheng, Yang Li, Junjie He, and Rui Feng. Mixtures of experts for audio-visual learning. In *NeurIPS*, pp. 1–25, 2024.
- Jean-Baptiste Cordonnier, Andreas Loukas, and Martin Jaggi. On the relationship between self-attention and convolutional layers. In *ICLR*, 2020.

- Haiwen Diao, Bo Wan, Xu Jia, Yunzhi Zhuge, Ying Zhang, Huchuan Lu, and Long Chen. Sherl: Synthesizing high accuracy and efficient memory for resource-limited transfer learning. In *ECCV*, pp. 75–95. Springer, 2024a.
- Haiwen Diao, Bo Wan, Ying Zhang, Xu Jia, Huchuan Lu, and Long Chen. Unipt: Universal parallel tuning for transfer learning with efficient parameter and memory. In *CVPR*, pp. 28729–28740, 2024b.
- Alexey Dosovitskiy. An image is worth 16x16 words: Transformers for image recognition at scale. In *ICLR*, 2021.
- Haoyi Duan, Yan Xia, Zhou Mingze, Li Tang, Jieming Zhu, and Zhou Zhao. Cross-modal prompts: Adapting large pre-trained models for audio-visual downstream tasks. In *NeurIPS*, pp. 1–20, 2024.
- Junyu Gao, Mengyuan Chen, and Changsheng Xu. Collecting cross-modal presence-absence evidence for weakly-supervised audio-visual event perception. In *CVPR*, pp. 18827–18836, 2023a.
- Kaifeng Gao, Long Chen, Hanwang Zhang, Jun Xiao, and Qianru Sun. Compositional prompt tuning with motion cues for open-vocabulary video relation detection. *arXiv preprint arXiv:2302.00268*, 2023b.
- Shengyi Gao, Zhe Chen, Guo Chen, Wenhai Wang, and Tong Lu. Avsegformer: Audio-visual segmentation with transformer. In *AAAI*, pp. 12155–12163, 2024.
- Jort F Gemmeke, Daniel PW Ellis, Dylan Freedman, Aren Jansen, Wade Lawrence, R Channing Moore, Manoj Plakal, and Marvin Ritter. Audio set: An ontology and human-labeled dataset for audio events. In *ICASSP*, pp. 776–780, 2017.
- Amin Ghiasi, Hamid Kazemi, Eitan Borgnia, Steven Reich, Manli Shu, Micah Goldblum, Andrew Gordon Wilson, and Tom Goldstein. What do vision transformers learn? a visual exploration. *arXiv preprint arXiv:2212.06727*, 2022.
- Aidan N Gomez, Mengye Ren, Raquel Urtasun, and Roger B Grosse. The reversible residual network: Backpropagation without storing activations. In *NeurIPS*, 2017.
- Yuxian Gu, Xu Han, Zhiyuan Liu, and Minlie Huang. Ppt: Pre-trained prompt tuning for few-shot learning. *arXiv preprint arXiv:2109.04332*, 2021.
- Cunhan Guo, Heyan Huang, and Yanghao Zhou. Enhance audio-visual segmentation with hierarchical encoder and audio guidance. *Neurocomputing*, pp. 1–10, 2024a.
- Ruohao Guo, Liao Qu, Dantong Niu, Yanyu Qi, Wenzhen Yue, Ji Shi, Bowei Xing, and Xianghua Ying. Open-vocabulary audio-visual semantic segmentation. In *ACM MM*, pp. 7533–7541, 2024b.
- Ruohao Guo, Xianghua Ying, Yaru Chen, Dantong Niu, Guangyao Li, Liao Qu, Yanyu Qi, Jinxing Zhou, Bowei Xing, Wenzhen Yue, et al. Audio-visual instance segmentation. In *CVPR*, pp. 13550–13560, 2025.
- Neil Houlsby, Andrei Giurgiu, Stanislaw Jastrzebski, Bruna Morrone, Quentin De Laroussilhe, Andrea Gesmundo, Mona Attariyan, and Sylvain Gelly. Parameter-efficient transfer learning for nlp. In *ICML*, pp. 2790–2799. PMLR, 2019.
- Di Hu, Rui Qian, Minyue Jiang, Xiao Tan, Shilei Wen, Errui Ding, Weiyao Lin, and Dejing Dou. Discriminative sounding objects localization via self-supervised audiovisual matching. In *NeurIPS*, pp. 10077–10087, 2020.

- Edward J Hu, Yelong Shen, Phillip Wallis, Zeyuan Allen-Zhu, Yuezhi Li, Shean Wang, Lu Wang, and Weizhu Chen. Lora: Low-rank adaptation of large language models. *arXiv preprint arXiv:2106.09685*, 2021.
- Siteng Huang, Biao Gong, Yulin Pan, Jianwen Jiang, Yiliang Lv, Yuyuan Li, and Donglin Wang. Vop: Text-video co-operative prompt tuning for cross-modal retrieval. In *CVPR*, pp. 6565–6574, 2023.
- Menglin Jia, Luming Tang, Bor-Chun Chen, Claire Cardie, Serge Belongie, Bharath Hariharan, and Ser-Nam Lim. Visual prompt tuning. In *ECCV*, pp. 709–727, 2022.
- Rabeeh Karimi Mahabadi, James Henderson, and Sebastian Ruder. Compacter: Efficient low-rank hypercomplex adapter layers. In *NeurIPS*, pp. 1022–1035, 2021.
- Muhammad Uzair Khattak, Hanoona Rasheed, Muhammad Maaz, Salman Khan, and Fahad Shahbaz Khan. Maple: Multi-modal prompt learning. In *CVPR*, pp. 19113–19122, 2023a.
- Muhammad Uzair Khattak, Syed Talal Wasim, Muzammal Naseer, Salman Khan, Ming-Hsuan Yang, and Fahad Shahbaz Khan. Self-regulating prompts: Foundational model adaptation without forgetting. In *ICCV*, pp. 15190–15200, 2023b.
- Jongsuk Kim, Jiwon Shin, and Junmo Kim. Avcap: Leveraging audio-visual features as text tokens for captioning. *arXiv preprint arXiv:2407.07801*, 2024.
- Yung-Hsuan Lai, Yen-Chun Chen, and Frank Wang Yu-Chiang. Modality-independent teachers meet weakly-supervised audio-visual event parser. In *NeurIPS*, pp. 1–19, 2023.
- Brian Lester, Rami Al-Rfou, and Noah Constant. The power of scale for parameter-efficient prompt tuning. *arXiv preprint arXiv:2104.08691*, 2021.
- Guangyao Li, Yake Wei, Yapeng Tian, Chenliang Xu, Ji-Rong Wen, and Di Hu. Learning to answer questions in dynamic audio-visual scenarios. In *CVPR*, pp. 19108–19118, 2022.
- Guangyao Li, Wenxuan Hou, and Di Hu. Progressive spatio-temporal perception for audio-visual question answering. In *ACM MM*, pp. 7808–7816, 2023a.
- Guangyao Li, Henghui Du, and Di Hu. Boosting audio visual question answering via key semantic-aware cues. In *ACM MM*, pp. 5997–6005, 2024a.
- Kexin Li, Zongxin Yang, Lei Chen, Yi Yang, and Jun Xiao. Catr: Combinatorial-dependence audio-queried transformer for audio-visual video segmentation. In *ACM MM*, pp. 1485–1494, 2023b.
- Xiang Lisa Li and Percy Liang. Prefix-tuning: Optimizing continuous prompts for generation. *arXiv preprint arXiv:2101.00190*, 2021.
- Zhangbin Li, Dan Guo, Jinxing Zhou, Jing Zhang, and Meng Wang. Object-aware adaptive-positivity learning for audio-visual question answering. In *AAAI*, pp. 3306–3314, 2024b.
- Zhangbin Li, Jinxing Zhou, Jing Zhang, Shengeng Tang, Kun Li, and Dan Guo. Patch-level sounding object tracking for audio-visual question answering. In *AAAI*, pp. 5075–5083, 2025.
- Yan-Bo Lin and Yu-Chiang Frank Wang. Audiovisual transformer with instance attention for audio-visual event localization. In *ACCV*, 2020.

- Yan-Bo Lin, Yu-Jhe Li, and Yu-Chiang Frank Wang. Dual-modality seq2seq network for audio-visual event localization. In *ICASSP*, pp. 2002–2006, 2019.
- Yan-Bo Lin, Yi-Lin Sung, Jie Lei, Mohit Bansal, and Gedas Bertasius. Vision transformers are parameter-efficient audio-visual learners. In *CVPR*, pp. 2299–2309, 2023.
- Jinxiang Liu, Yikun Liu, Fei Zhang, Chen Ju, Ya Zhang, and Yanfeng Wang. Audio-visual segmentation via unlabeled frame exploitation. In *CVPR*, pp. 26328–26339, 2024.
- Xu Liu, Na Xia, Jinxing Zhou, Zhangbin Li, and Dan Guo. Towards energy-efficient audio-visual classification via multimodal interactive spiking neural network. *ACM Transactions on Multimedia Computing, Communications and Applications*, 21(5):1–24, 2025.
- Ze Liu, Han Hu, Yutong Lin, Zhuliang Yao, Zhenda Xie, Yixuan Wei, Jia Ning, Yue Cao, Zheng Zhang, Li Dong, et al. Swin transformer v2: Scaling up capacity and resolution. In *CVPR*, pp. 12009–12019, 2022.
- Juncheng Ma, Peiwen Sun, Yaoting Wang, and Di Hu. Stepping stones: a progressive training strategy for audio-visual semantic segmentation. In *ECCV*, pp. 311–327. Springer, 2024.
- Tanvir Mahmud, Shentong Mo, Yapeng Tian, and Diana Marculescu. Ma-avt: Modality alignment for parameter-efficient audio-visual transformers. *arXiv preprint arXiv:2406.04930*, 2024a.
- Tanvir Mahmud, Yapeng Tian, and Diana Marculescu. T-vsl: Text-guided visual sound source localization in mixtures. In *CVPR*, pp. 26742–26751, 2024b.
- Yuxin Mao, Xuyang Shen, Jing Zhang, Zhen Qin, Jinxing Zhou, Mochu Xiang, Yiran Zhong, and Yuchao Dai. Tavgbench: Benchmarking text to audible-video generation. In *ACM MM*, pp. 6607–6616, 2024.
- Paulius Micikevicius, Sharan Narang, Jonah Alben, Gregory Diamos, Erich Elsen, David Garcia, Boris Ginsburg, Michael Houston, Oleksii Kuchaiev, Ganesh Venkatesh, et al. Mixed precision training. *arXiv preprint arXiv:1710.03740*, 2017.
- Shentong Mo and Yapeng Tian. Multi-modal grouping network for weakly-supervised audio-visual video parsing. In *NeurIPS*, pp. 1–12, 2022.
- Sungho Park and Hyeran Byun. Fair-vpt: Fair visual prompt tuning for image classification. In *CVPR*, pp. 12268–12278, 2024.
- Maithra Raghu, Thomas Unterthiner, Simon Kornblith, Chiyuan Zhang, and Alexey Dosovitskiy. Do vision transformers see like convolutional neural networks? In *NeurIPS*, pp. 12116–12128, 2021.
- Varshanth Rao, Md Ibrahim Khalil, Haoda Li, Peng Dai, and Juwei Lu. Dual perspective network for audio-visual event localization. In *ECCV*, pp. 689–704, 2022.
- Shuvendu Roy and Ali Etemad. Consistency-guided prompt learning for vision-language models. *arXiv preprint arXiv:2306.01195*, 2023.
- Faegheh Sardari, Armin Mustafa, Philip JB Jackson, and Adrian Hilton. Coleaf: A contrastive-collaborative learning framework for weakly supervised audio-visual video parsing. In *ECCV*, pp. 1–17, 2024.
- Xuyang Shen, Dong Li, Jinxing Zhou, Zhen Qin, Bowen He, Xiaodong Han, Aixuan Li, Yuchao Dai,

- Lingpeng Kong, Meng Wang, et al. Fine-grained audible video description. In *CVPR*, pp. 10585–10596, 2023.
- Yi-Lin Sung, Jaemin Cho, and Mohit Bansal. Lst: Ladder side-tuning for parameter and memory efficient transfer learning. In *NeurIPS*, pp. 12991–13005, 2022.
- Yapeng Tian, Chenxiao Guan, Justin Goodman, Marc Moore, and Chenliang Xu. An attempt towards interpretable audio-visual video captioning. *arXiv preprint arXiv:1812.02872*, 2018a.
- Yapeng Tian, Jing Shi, Bochen Li, Zhiyao Duan, and Chenliang Xu. Audio-visual event localization in unconstrained videos. In *ECCV*, pp. 247–263, 2018b.
- Yapeng Tian, Chenxiao Guan, Justin Goodman, Marc Moore, and Chenliang Xu. Audio-visual interpretable and controllable video captioning. In *CVPR Workshops*, 2019.
- Yapeng Tian, Dingzeyu Li, and Chenliang Xu. Unified multisensory perception: Weakly-supervised audio-visual video parsing. In *ECCV*, pp. 436–454, 2020.
- Ashish Vaswani, Noam Shazeer, Niki Parmar, Jakob Uszkoreit, Llion Jones, Aidan N Gomez, Łukasz Kaiser, and Illia Polosukhin. Attention is all you need. In *NeurIPS*, pp. 1–11, 2017.
- Kai Wang, Yapeng Tian, and Dimitrios Hatzinakos. Towards efficient audio-visual learners via empowering pre-trained vision transformers with cross-modal adaptation. In *CVPR Workshop*, pp. 1837–1846, 2024a.
- Naigang Wang, Jungwook Choi, Daniel Brand, Chia-Yu Chen, and Kailash Gopalakrishnan. Training deep neural networks with 8-bit floating point numbers. In *NeurIPS*, 2018.
- Zhen Wang, Jun Xiao, Yueting Zhuang, Fei Gao, Jian Shao, and Long Chen. Learning combinatorial prompts for universal controllable image captioning. *IJCV*, pp. 1–22, 2024b.
- Yake Wei, Di Hu, Yapeng Tian, and Xuelong Li. Learning in audio-visual context: A review, analysis, and new perspective. *arXiv preprint arXiv:2208.09579*, 2022.
- Yu Wu and Yi Yang. Exploring heterogeneous clues for weakly-supervised audio-visual video parsing. In *CVPR*, pp. 1326–1335, 2021.
- Yan Xia and Zhou Zhao. Cross-modal background suppression for audio-visual event localization. In *CVPR*, pp. 19989–19998, 2022.
- Saining Xie, Ross Girshick, Piotr Dollár, Zhuowen Tu, and Kaiming He. Aggregated residual transformations for deep neural networks. In *CVPR*, pp. 1492–1500, 2017.
- Haoming Xu, Runhao Zeng, Qingyao Wu, Mingkui Tan, and Chuang Gan. Cross-modal relation-aware networks for audio-visual event localization. In *ACM MM*, pp. 3893–3901, 2020.
- Jiarui Xu, Shalini De Mello, Sifei Liu, Wonmin Byeon, Thomas Breuel, Jan Kautz, and Xiaolong Wang. Groupvit: Semantic segmentation emerges from text supervision. In *CVPR*, pp. 18134–18144, 2022.
- Lingfeng Yang, Yuezhe Wang, Xiang Li, Xinlong Wang, and Jian Yang. Fine-grained visual prompting. In *NeurIPS*, 2024.
- Hantao Yao, Rui Zhang, and Changsheng Xu. Tcpc: Textual-based class-aware prompt tuning for visual-language model. In *CVPR*, pp. 23438–23448, 2024.

- Jiashuo Yu, Ying Cheng, Rui-Wei Zhao, Rui Feng, and Yuejie Zhang. MM-Pyramid: Multimodal pyramid attentional network for audio-visual event localization and video parsing. In *ACM MM*, pp. 6241–6249, 2022.
- Heeseung Yun, Youngjae Yu, Wonsuk Yang, Kangil Lee, and Gunhee Kim. Pano-avqa: Grounded audio-visual question answering on 360deg videos. In *ICCV*, pp. 2031–2041, 2021.
- Chiyuan Zhang, Samy Bengio, and Yoram Singer. Are all layers created equal? *arXiv preprint arXiv:1902.01996*, 2022.
- Ji Zhang, Shihan Wu, Lianli Gao, Heng Tao Shen, and Jingkuan Song. Dept: Decoupled prompt tuning. In *CVPR*, pp. 12924–12933, 2024.
- Hang Zhao, Chuang Gan, Andrew Rouditchenko, Carl Vondrick, Josh McDermott, and Antonio Torralba. The sound of pixels. In *ECCV*, pp. 570–586, 2018.
- Pengcheng Zhao, Jinxing Zhou, Yang Zhao, Dan Guo, and Yanxiang Chen. Multimodal class-aware semantic enhancement network for audio-visual video parsing. In *AAAI*, pp. 10448–10456, 2025.
- Yihan Zhao, Wei Xi, Yuhang Cui, Gairui Bai, Xinhui Liu, and Jizhong Zhao. Copl:parameter-efficient collaborative prompt learning for audio-visual tasks. In *ACM MM*, pp. 4455–4464, 2024.
- Jinxing Zhou, Liang Zheng, Yiran Zhong, Shijie Hao, and Meng Wang. Positive sample propagation along the audio-visual event line. In *CVPR*, pp. 8436–8444, 2021.
- Jinxing Zhou, Dan Guo, and Meng Wang. Contrastive positive sample propagation along the audio-visual event line. *IEEE Transactions on Pattern Analysis and Machine Intelligence*, 45(6):7239–7257, 2022a.
- Jinxing Zhou, Jianyuan Wang, Jiayi Zhang, Weixuan Sun, Jing Zhang, Stan Birchfield, Dan Guo, Lingpeng Kong, Meng Wang, and Yiran Zhong. Audio-visual segmentation. In *ECCV*, pp. 386–403, 2022b.
- Jinxing Zhou, Dan Guo, Yiran Zhong, and Meng Wang. Improving audio-visual video parsing with pseudo visual labels. *arXiv preprint arXiv:2303.02344*, 2023a.
- Jinxing Zhou, Xuyang Shen, Jianyuan Wang, Jiayi Zhang, Weixuan Sun, Jing Zhang, Stan Birchfield, Dan Guo, Lingpeng Kong, Meng Wang, et al. Audio-visual segmentation with semantics. *arXiv preprint arXiv:2301.13190*, 2023b.
- Jinxing Zhou, Dan Guo, Yuxin Mao, Yiran Zhong, Xiaojun Chang, and Meng Wang. Label-anticipated event disentanglement for audio-visual video parsing. In *ECCV*, pp. 35–51, 2024a.
- Jinxing Zhou, Dan Guo, Yiran Zhong, and Meng Wang. Advancing weakly-supervised audio-visual video parsing via segment-wise pseudo labeling. *International Journal of Computer Vision*, 132(11):5308–5329, 2024b.
- Jinxing Zhou, Dan Guo, Ruohao Guo, Yuxin Mao, Jingjing Hu, Yiran Zhong, Xiaojun Chang, and Meng Wang. Towards open-vocabulary audio-visual event localization. In *CVPR*, pp. 8362–8371, 2025a.
- Kaiyang Zhou, Jingkang Yang, Chen Change Loy, and Ziwei Liu. Conditional prompt learning for vision-language models. In *CVPR*, pp. 16816–16825, 2022c.
- Yang-Hao Zhou, Heyan Huang, Cunhan Guo, Rong-Cheng Tu, Zeyu Xiao, Bo Wang, and Xian-Ling Mao.

Aloha: Adapting local spatio-temporal context to enhance the audio-visual semantic segmentation. *ACM Transactions on Multimedia Computing, Communications and Applications*, 2025b.

Ziheng Zhou, Jinxing Zhou, Wei Qian, Shengeng Tang, Xiaojun Chang, and Dan Guo. Dense audio-visual event localization under cross-modal consistency and multi-temporal granularity collaboration. In *AAAI*, pp. 10905–10913, 2025c.

Jiawen Zhu, Simiao Lai, Xin Chen, Dong Wang, and Huchuan Lu. Visual prompt multi-modal tracking. In *CVPR*, pp. 9516–9526, 2023.